Highly Selective Molybdenum-Based Catalysts for Ring Hydrogenation and Contraction

*Ali Mehdad,[a] Rolf E. Jentoft,[b] and Friederike C. Jentoft[b]**

[a]School of Chemical, Biological & Materials Engineering, University of Oklahoma, Norman

[b]Department of Chemical Engineering, University of Massachusetts Amherst

*corresponding author mailing address: Dept. of Chemical Engineering, University of Massachusetts Amherst, 686 N Pleasant, Amherst, MA 01003; Email: fcjentoft@umass.edu

Abstract

The reduction and carburization of oxides of molybdenum, tungsten, niobium, and selected mixed oxides of the same elements in H_2/hydrocarbon atmospheres were investigated with the goal of generating non-noble metal catalysts capable of aromatic ring hydrogenation and contraction. Toluene served as a surrogate for heavy aromatics and as a diagnostic reactant for the nature of the surface sites. At 400 °C, a H_2:toluene molar ratio of 35:1, and a total pressure of 21 bar, all oxides except Nb_2O_5 were converted into active catalysts that produced methyl-cyclohexane, ethylcyclopentane, dimethylcyclopentane, benzene and xylene, and C1-C6 alkanes. Increasing hydrogenolysis selectivity with time on stream indicated slow carbide formation. At 350 °C, MoO_3 was converted into a stable catalyst with about 35% and 55% carbon selectivity to methylcyclohexane and ring contraction products, respectively, and little C1-C6 formation. Selectivity was largely invariant to conversion. Post-reaction analysis of this material by powder diffraction indicated a mixture of MoO_2 and a second phase characterized by cubic symmetry, which, while the sample contained a small amount of carbon, was best described as oxidic with a metal-to-oxygen ratio of roughly 1:2. Oxides containing two metal cations showed shorter induction periods and better long-term stability than MoO_3, revealing further potential for optimization of this type of catalyst.

Keywords: MoO_3; MoO_2; oxycarbide; thermal analysis; hydroconversion; bifunctional

1. Introduction

Ring contraction of alicyclic hydrocarbons is a useful step in the conversion of polycyclic aromatic compounds – which are major ingredients in oil sands[1] and some refinery streams such as light cycle oil[2] – to gasoline or diesel fuels. In principle, only ring hydrogenation and ring opening are required, but it has been found that 5-membered rings open more easily than 6-membered rings.[3] While ring hydrogenation and ring opening by hydrogenolysis require a catalyst with metallic sites, ring contraction and ring opening by cracking require a catalyst with acidic sites. Consequently, catalysts for ring opening combine both functions and typically consist of a metal such as iridium or platinum supported on solids acids such as alumina, zeolite beta, or zeolite Y.[3,4] However, the sulfur sensitivity of noble metals presents a problem.[1] A more robust alternative to supported metals could be transition metal oxycarbide catalysts, which have also been reported to show metal-acidic bifunctional character.

Transition metal carbides are known to have catalytic properties similar to those of noble metals for some reactions.[5,6] This behavior has been explained with a hybridization between the *p* orbitals of the carbon and the *d* orbitals of the metal and the associated change in the d-band structure of the metal.[7] According to DFT calculations, addition of oxygen to metal carbide surfaces reduces their affinity to carbon, oxygen, and hydrogen,[8] and, consistent with this property change, it has been experimentally found that hydrogenation and hydrogenolysis activities of carbides are lower when oxygen is present on their surfaces[9-13] and that at the same time, transformations typical of Brønsted acid sites and carbenium ion chemistry are observed.[9-11,1415]

Oxycarbides can be produced via partial oxidation of a carbide, or via partial carburization of an oxide. The most commonly investigated carbides, molybdenum and tungsten carbide readily react with O_2,[13] and consequently, O_2 is the primary reactant used to create oxygen-modified

carbides of tungsten[9-11] or molybdenum.[15-18] Alternatively, in reactions of oxygenates, oxygen from the reactant may be retained. [19] Oxides have been found to partially or fully transform to carbides at the conditions of many of the catalytic reactions of interest, typically implying exposure to a mixed H_2/hydrocarbon atmosphere. For example, treatment of molybdenum oxides in a mixture of an alkane (*n*-butane,[20] *n*-hexane,[21,22] *n*-heptane[23]) and H_2 at a temperature of 350 °C resulted in oxycarbides, whereas treatment at 400 °C in toluene resulted in molybdenum carbides.[24,25] Evidence for the presence of oxygen on carbide surfaces or carbon on oxide surfaces largely comes from surface chemical analysis,[21,26] probe molecule adsorption, temperature-programmed experiments,[20] or an oxygen balance during catalysis.[19] If the transformation occurs during the catalytic process, characterization of the surface and bulk properties can be a challenge because of harsh conditions and transient behavior, and even post-reaction analysis can be hampered by the pyrophoric nature of the materials. Indeed, there are few reports demonstrating the formation of stoichiometric, bulk oxycarbides,[21,22] and even fewer reports of mixed oxycarbides of molybdenum or tungsten.[27,28]

Moreover, there are discrepancies in the literature regarding the nature of the active phase. The isomerization of alkanes including *n*-butane,[20] *n*-heptane, [29-31] *n*-octane,[31] the isomerization and dehydrogenation of *n*-butane,[32] and the hydrodeoxygenation of oxygenates[33] have been ascribed to the action of oxycarbides of molybdenum or tungsten. However, there are also a substantial number of reports in which similar conditions were used and the catalytic activity was ascribed to MoO_2 (2-methylpentane/H_2 at 350 °C,[34] *n*-heptane/H_2 at 300 °C[35]) or a hydrogen-containing MoO_xH_y phase (*n*-pentane/H_2 at 250 °C[36]).

This investigation focuses on combining molybdenum with a second metal, with the goal of tuning the relative fractions of metallic and acid sites on the surface of such multi-anion materials

while also stabilizing the material under catalytic operating conditions. Tungsten[13] and niobium[37] are selected, which retain oxygen more strongly than molybdenum. Well-defined mixed oxides are used as starting materials and are transformed under catalytic reaction conditions. Toluene is chosen as a surrogate reactant for polycyclic compounds as it can undergo all relevant transformations. It is demonstrated that molybdenum-containing catalysts can be tuned for a new application, aromatic ring hydrogenation with ring contraction, and that toluene conversion is an effective probe reaction that can distinguish between metallic sites and Brønsted acid sites of various strength.

2. Experimental section

2.1. Starting materials and oxide synthesis

Ammonium heptamolybdate (ACS reagent, 81-83% MoO_3, Sigma Aldrich), ammonium niobate (V) oxalate hydrate (99.99%, Aldrich), ammonium paratungstate (Alfa Aesar), MoO_3 (99.95%, Alfa Aesar) and WO_3 (99.995%, Aldrich) were used as starting materials for catalyst synthesis. Oxides that were charged to the test reactor were obtained by three different routes, as identified by a suffix. Commercial oxides were used as received (sample names ending -C). Oxides were also obtained through calcination of precursors containing a single or two intimately mixed metals cations. These precursors were produced by flash-freezing and subsequent freeze-drying (-FD), or through hydrothermal (-HT) synthesis. The details of the freeze-drying and hydrothermal syntheses are described elsewhere.[37]

All calcinations were conducted in and monitored by a thermogravimetric analyzer (TGA) connected to an online MS (Netzsch STA 449 F1 and QMS 403 C). The calcination gases were 80% air (zero grade, Airgas) in balance of argon (UHP, Airgas) with a total flow rate of 100 ml/min. All flow rates were at STP. Gases were purified; air was passed through a moisture trap

(Agilent, MT400-2) and argon was passed through a dual trap of moisture and oxygen (Z-Pure Dual Purifier). The synthesis of oxides was carried out at atmospheric pressure by heating from 40 °C to the final calcination temperature with a ramp of 5 °C/min and holding at that final temperature for 30 min. Molar ratios of CO to H_2O were estimated using ionization cross sections and fragmentation patterns at 70 eV ionization energy (NIST).

2.2. Carburization of oxides in a mixture of methane and H_2 at atmospheric pressure

Carburizations at atmospheric pressure were performed in the thermogravimetric analyzer described in Section 2.1. The carburization gas was a mixture of 20% CH_4, 70% H_2 and 10% Ar and was supplied at a total flow rate of 100 ml/min. The heating rate was 5 °C/min to 450 °C and then 2 °C/min to the final carburization temperature.

2.3. Carburization in toluene and catalytic conversion of toluene

The carburization of oxides and the vapor phase conversion of toluene were conducted in a ¼ inch stainless steel packed bed flow reactor previously described in detail.[13] For synthesis and reactions at 400 °C, the reactor was loaded with about 48 mg of oxide catalyst precursor giving a W/F of about 0.185 h based on the oxide weight. For synthesis and reaction experiments at 350 °C, the oxide weight and toluene flow rate were varied to give weight hourly space velocities between 0.04 and 2.4 h. The oxide sample was mixed with about 400 mg of SiC (Aldrich, 200-450 mesh) to avoid channeling and local heating. The feed was 0.005 ml/min of liquid toluene (99.5%, Mallinckrodt Chemicals) and 38 ml/min STP H_2 (Ultra high purity, Airgas). The reactor pressure was controlled by a back-pressure valve. The reactor was first pressurized to an absolute pressure of 21 bar with H_2, and then toluene was added to the feed. The reactor contents were heated to 110 °C applying a temperature ramp of 5 °C/min while flowing a mixture of toluene and H_2. When the toluene flow reached steady state, the temperature was increased to 400 or 350 °C

with a ramp of 5 °C /min and was then held for 24 to 96 h. The effluent stream was analyzed using an OmniStar GSD 320 mass spectrometer and an HP 5890 GC with flame ionization detector (FID), equipped with a 30 m, 0.32 mm GASPRO column. The GC temperature program was: 5 min isothermal at 60 °C, then a ramp at 10 °C/min to a final temperature of 240 °C, which was held for 4 min. MS and GC data times are corrected by 4.4 minutes for the volume of gas between the catalyst bed and the GC and MS sampling points.

Conversion of toluene X in % is defined by Eq. 1:

$$X = \frac{(\text{number of moles of toluene in feed} - \text{number of moles of toluene in effluent}) \times 100\%}{\text{number of moles of toluene in feed}} \quad (1)$$

The selectivity S of compound i in % was calculated using Eq. 2:

$$S = \frac{(\text{number of moles of compound } i) \times (\text{number of carbon atoms in compound } i) \times 100\%}{\sum_{j=1}^{n} (\text{number of moles of product } j) \times (\text{number of carbon atoms in compound } j)}. \quad (2)$$

The average rate of toluene consumption r was calculated from toluene conversion X and toluene molar flow rate $F_{Toluene}$ according to Eq. 3. The rate was normalized to the moles of metal present in the reactor by accounting for the molecular weight of the oxide and the number of metal atoms per formula unit, υ.

$$r = \frac{X_{Toluene}}{100\%} \times F_{Toluene} \frac{MW_{Oxide}}{m_{Oxide} \times v} \quad (3)$$

Materials designated for characterization by N_2 adsorption, scanning electron microscopy (SEM), or X-ray diffraction (XRD) were passivated before removal from the reactor by slow admission of air to the reactor.

2.4. Materials characterization

The carbon content of spent catalysts was determined in situ by temperature-programmed oxidation (TPO), and the surface was probed for acid sites with nitrogen bases. The catalytic reactor was depressurized, purged with argon or N_2 overnight, and set to the desired temperature. The starting temperature for TPO experiments was 20 °C, and the sample was heated in a 50 ml/min flow of 20% O_2 in N_2 at a ramp rate of 10 °C/min until a final temperature of 550 °C. The effluent was analyzed by MS (Pfeiffer Omnistar), and the signal at m/z =44 divided by the signal for m/z = 28 was used to monitor CO_2 formation. MS intensity was calibrated by decomposing a known amount of $CaCO_3$ (Fisher, 99.5 %).

Scanning electron microscopy was performed with a FEI Magellan 400 XHR instrument that was equipped with a field emission gun and operated at 3.0 kV.

The bulk structure of the materials was characterized by X-ray diffraction using a Rigaku Ultima IV instrument with Cu Kα radiation, a D/tex detector and Bragg Brentano optical configuration. The X-ray source was operated at 40 kV and 44 mA. The diffractograms were collected over a 2θ range of 10 to 70°. The diffractograms were fit to reported structures using Powdercell software.

BET surface areas were measured using a Micromeritics ASAP 2020 and N_2 at a temperature of -196 °C. Before measuring the surface areas, the samples were degassed at a temperature of 200 °C for 4 h. Pore size distributions were determined from the desorption branch of N_2 desorption isotherms by applying the BJH method.

To characterize acid sites, nitrogen bases 2,6-dimethylpyridine (2,6-lutidine, Fisher, 99%), acetonitrile (Fisher, 99.9%), and isopropylamine (Aldrich, 99.5%) were used. The bases were introduced in pulses of 1 µl of liquid, which vaporized in the hot feed line, until saturation was

reached. The pulse size corresponds to 8.9 μmol lutidine, 19.1 μmol acetonitrile, and 11.6 μmol isopropylamine; and sorption temperatures were 150 °C, 100 °C, and 50 °C, respectively. The amount adsorbed was monitored by MS, which was calibrated by determining the area under a pulse of a known amount of the same base. For temperature-programmed desorption (TPD) of the probes, the samples were heated in N_2 flow of 50 ml/min at a rate of 10 °C/min. Desorption was monitored by MS. During the thermal decomposition of the adsorbed isopropylamine, propylene formation was monitored at m/z=41 by MS. The concentration was determined through single-point simultaneous injection into a GC (Varian 3800) with flame ionization detection that was calibrated by injecting an alkene mixture of known composition.

3. Results

3.1. Synthesis and characterization of oxides

The precursor materials were calcined at the lowest temperature that resulted in complete conversion to the oxides, to optimize surface area and avoid sublimation of MoO_3. Calcination was monitored by TG-MS, and the criteria for completion were constant sample weight and no evolution of gas phase products. Compositions, final calcination temperatures and textural properties are reported in Table 1. The metal ratio in mixed oxides corresponds to the starting ratio for freeze-dried materials, whereas EDS analysis was used for hydrothermally obtained materials, since the obtained solids are enriched in niobium relative to the synthesis solution.[37] Oxygen contents are calculated assuming fully oxidized metals.

The freeze-dried and calcined ammonium heptamolybdate (MoO_3–FD) and ammonium paratungstate (WO_3–FD) had higher surface areas than the commercial oxides. Oxides prepared by calcination of hydrothermally synthesized precursors, $Mo_{0.66}Nb_{0.34}O_{2.83}$-HT and Nb_2O_5-HT,

had higher surface areas compared to the oxides prepared by calcination of freeze-dried precursors. Among all oxides, Nb_2O_5 had the highest surface area (42.9 m^2/g).

Table 1: Oxide sample calcination temperatures and N_2 sorption characterization results.

Sample	Calcination final temperature (°C)	Oxide surface area (m^2/g)	BJH desorption pore diameter (Å)	BJH desorption pore volume (cm^3/g)
MoO_3-FD	450	7.0	123	0.023
MoO_3-C	NA	0.3	78	0.0004
WO_3-FD	500	7.6	120	0.022
WO_3-C	NA	1.6	271	0.010
$Mo_{0.5}W_{0.5}O_3$-FD	450	2.8	85	0.005
$Mo_{0.86}Nb_{0.14}O_{2.93}$-FD	450	14.9	124	0.051
$Mo_{0.66}Nb_{0.34}O_{2.83}$-HT	450	26.5	200	0.142
Nb_2O_5-HT	600	42.9	165	0.21

3.2. Carburization of oxides at atmospheric pressure in CH_4/H_2

To establish a link to published carburization data and to create a reference point for MS data collected during reduction and possible carbide formation in a mixture of toluene and H_2 at high pressure, the calcined oxides were carburized in a mixture of methane and H_2 at atmospheric pressure, and the transformations were monitored by TG-MS. The mass charge ratios (m/z) 18 and 28 are shown to demonstrate the formation of H_2O and CO. Other m/z ratios (2, 15) were analyzed but provided only limited additional insight: H_2 consumption mirrored H_2O formation, and methane consumption was insignificant and thus not detectable. The profiles in Figure 1 differ significantly in various respects. The transformation of the MoO_3 sample to Mo_2C was characterized by two reduction steps approximately corresponding to removal of first one and then two oxygens, respectively, as can be seen from the weight loss and the relative size of the two

water peaks. Less than 10% of the oxygen evolved as carbon monoxide in a very sharp peak at about 600 °C. In contrast, WO_3 first lost two oxygens and then one; and less than 5% of the oxygen was lost as CO concomitantly with the second water peak. There was also a minimum in mass, indicating deep reduction of tungsten. The mixed oxides $Mo_{0.5}W_{0.5}O_3$ and $Mo_{0.86}Nb_{0.14}O_{2.93}$ behaved like MoO_3 in that the first reduction steps, which were considered to be concluded at 550 °C and 450 °C, correspond to the loss of about one oxygen per metal. However, a significant fraction of oxygen was lost as CO, estimated to amount to 25% for $Mo_{0.5}W_{0.5}O_3$ and to 16-20% for $Mo_{0.86}Nb_{0.14}O_{2.93}$. The flat sections in the TG profile after the gas evolution ceases indicate completion of carbide formation for all four samples. The reduction of Nb_2O_5 (data shown in Ref. [37]) started only at 600 °C, and close to 80 % of the oxygen evolved as CO at 950 °C.

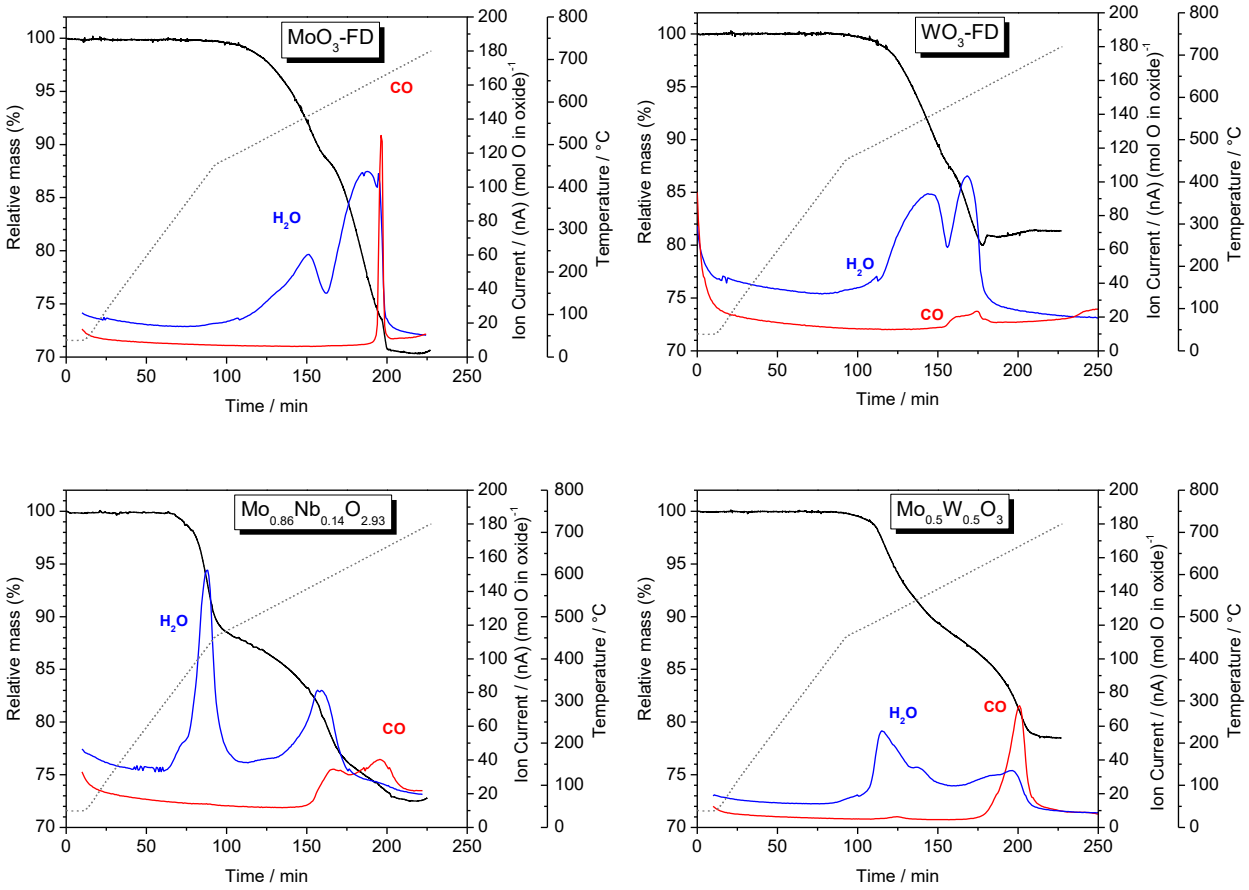

Figure 1: TG and MS (m/z=18 for H_2O and m/z=28 for CO) traces recorded during the carburization of selected oxides from Table 1 (all obtained by calcining freeze-dried materials) in a flow of 20% CH_4 / 70% H_2 /10% Ar. MS normalized to initial oxygen content of sample. Black solid line is relative mass (left axis), dotted line is temperature (far right axis).

3.3. Reduction of oxides at 21 bar in toluene/H_2

Reduction in the reactant mixture was conducted in the steel reactor, and the gas phase products were monitored by online MS. Figure 2a shows the evolution of H_2O (m/z=18) for pure and mixed oxides during a period of 100 min while the sample was heated to 400 °C. Nb_2O_5 was not reduced under these conditions. All other samples started reducing much earlier than at atmospheric pressure (cf. Figure 1); the molybdenum-niobium samples ($Mo_{0.86}Nb_{0.14}O_{2.93}$-FD and $Mo_{0.66}Nb_{0.34}O_{2.83}$-HT) started at 200 °C, MoO_3-FD and $Mo_{0.5}W_{0.5}O_3$-FD at 275 °C, and WO_3 at about 350 °C. Reduction of all mixed metal oxides occurred over a wide temperature span and

continued after the maximum temperature was reached. The data were normalized to the initial oxygen content of the samples, and hence relative areas reflect relative degrees of reduction. Within the accuracy of the method, the molybdenum-containing samples in Figure 2 were equally reduced, since the peak areas were between 90 and 110% of that measured for MoO_3. In contrast, WO_3 was much less reduced with a peak area of only 20% of that of MoO_3. The data in Figure 2b demonstrate that the effect of temperature on the degree of reduction was small; at a final temperature of 350 °C, the degree of reduction of MoO_3-FD was 82% of that at a final temperature of 400 °C. In contrast, as also seen in Figure 2b, the effect of particle size was significant. The commercial sample MoO_3-C had a much lower surface area than MoO_3-FD (Table 1). Consistently, the water peak for the commercial MoO_3 reached a maximum about 10 min after the reactor reached 350 °C, and the area was only 32% of that seen for MoO_3-FD during a ramp to 400 °C.

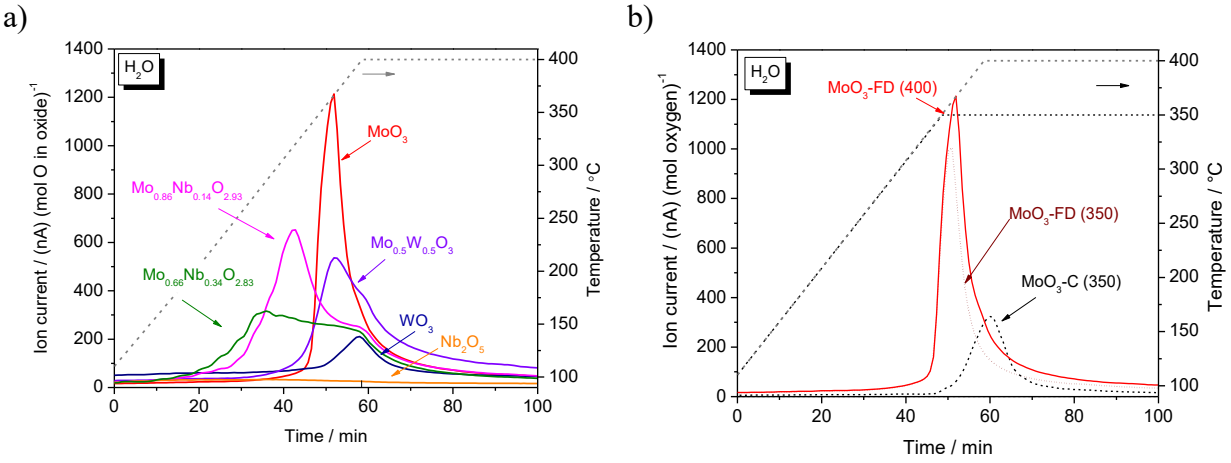

Figure 2: Water formation (m/z=18) during temperature-programmed reduction of oxides from 110 to 400 °C at 5 °C /min. Feed: 0.005 ml/min of liquid toluene and 38 ml/min of H_2, 21 bar. MS normalized to initial oxygen content of sample. (a) Effect of composition; samples are those listed in Table 1, with FD samples selected for MoO_3 and WO_3. (b) Effect of precursor particle size and final temperature on reduction of MoO_3.

To check for possible oxidation of toluene, m/z = 28 and 44 were also monitored. With the exception of MoO_3, for which a small peak of CO was observed concomitantly with the formation

of water at 350 °C, no significant amounts of CO or CO_2 were produced by the molybdenum-containing samples before the signals at m/z=28 and 44 were obscured through the onset of ethane and propane formation.

3.4. Toluene conversion and post-reaction catalyst analysis

3.4.1. Toluene vapor phase reaction in H_2 at 400 °C and preliminary tests at lower temperatures

In Figure 3a, the rate of toluene conversion at 400 °C is reported vs. time on stream. There was an induction period for all samples. After about 3 h at 400 °C, the mixed metal oxides reached a constant conversion; however, the pure oxides MoO_3 and WO_3 continued to gain activity over 24 h. After 24 h, Nb_2O_5 was still inactive and MoO_3 was the most active material. With increasing niobium content, materials became less active. The samples were pyrophoric when removed from the reactor, except for Nb_2O_5.

All active materials eventually yielded short-chain alkanes, methylcyclohexane, ethylcyclopentane, dimethylcyclopentane, benzene, and xylene. Alkanes were mainly methane and ethane, except for a brief period at early time on stream, when C3 and C4 alkanes prevailed for the molybdenum-containing materials. Consistent with the rapid approach to steady state, product selectivities did not change much for the mixed oxides $Mo_{0.5}W_{0.5}O_3$ and $Mo_{0.86}Nb_{0.14}O_{2.93}$ with time on stream, with ring contraction products ethylcyclopentane and dimethylcyclopentane making up about 55-65% and C1-C6 alkanes being significant at 15-20%. Pronounced trends in product selectivity (Figure 3b) were observed for the two pure oxides; the WO_3-derived material produced almost exclusively methylcyclohexane in the first few hours before other products were formed, whereas the MoO_3-derived material very early on stream produced all products listed above. Both materials produced increasing amounts of C1-C6 alkanes later on stream, but differed

with respect to selectivity toward five-membered rings, which was decreasing for MoO_3 and increasing for WO_3. Moreover, the selectivity of WO_3 became stable, whereas MoO_3 continued to produce increasing amounts of short chain alkanes. Average conversions and product selectivities during the last four hours of reaction are reported in Table 2.

(a)

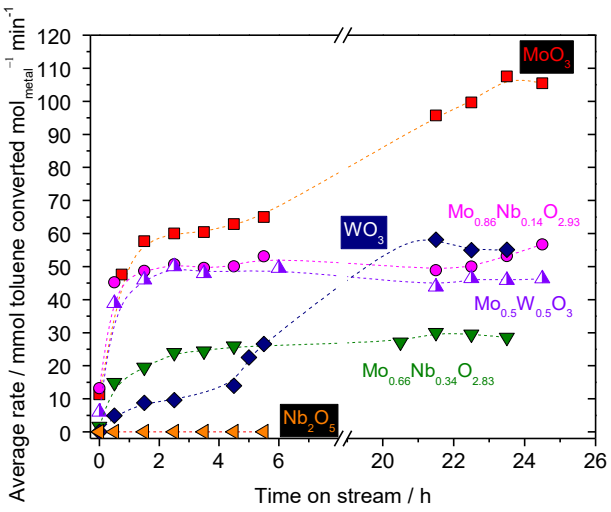

(b)

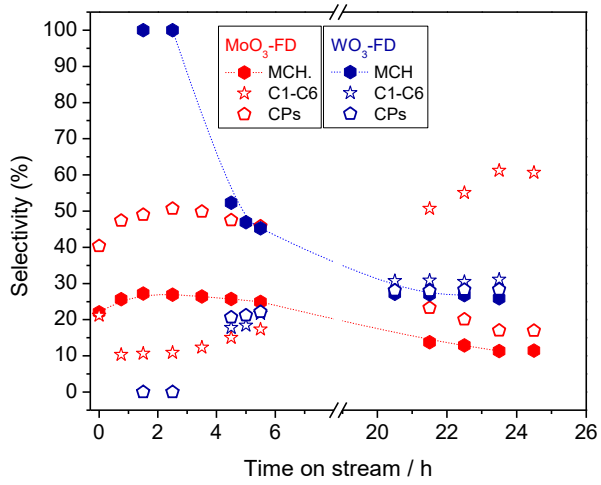

Figure 3: Toluene conversion at 400 °C after 5 °C/min temperature ramp in feed. (a) rate of toluene conversion; (b) carbon-based selectivity evolution for selected samples. Feed: 0.005 ml/min of liquid toluene and 38 ml/min of H_2, 21 bar. Mixed oxides are those listed in Table 1; MoO_3 is FD as is WO_3. At 0 h on stream, the reactor temperature had reached 400 °C. Conversion range up to 80% (MoO_3) or 40% (all other samples). Rate normalized to metal content.

The two most active materials, MoO_3 and $Mo_{0.86}Nb_{0.14}O_{2.93}$ were selected for further testing. Milder conditions were targeted to curb C-C cleavage to short-chain products and promote phase

stability. Preliminary experiments with $Mo_{0.86}Nb_{0.14}O_{2.93}$ showed toluene conversion to be low (*i.e.*, less than 10%) at activation temperatures of less than 350 °C, even though reduction can be initiated at 250 °C (cf. Figure 2). Further tests were thus conducted at 350 °C.

Table 2: Product selectivity of toluene conversion at 400 °C and 21 bar

Sample	Synthesis Method	Mass[a] (mg)	Conv.[b] (%)	Selectivity[b,c] (C%)					
				C1-C6	MCH	ECP	DMCP	Benzene	Xylene
MoO_3	FD	53.0	37.1	12.7	28.1	36.3	11.7	7.3	12.7
MoO_3	FD	48.5	73.1	56.9	12.4	15.1	4.3	8.4	3.0
WO_3	FD	49.5	25.7	30.8	26.7	16.7	11.5	11.3	3.0
$Mo_{0.5}W_{0.5}O_3$	FD	48.1	24.8	16.3	24.7	33.6	11.8	8.4	5.2
$Mo_{0.86}Nb_{0.14}O_{2.93}$	FD	48.5	37.9	18.1	22.9	31.9	11.1	11.4	4.6
$Mo_{0.66}Nb_{0.34}O_{2.83}$	HT	46.1	20.2	14.8	28.5	24.9	15.1	10.5	6.3
Nb_2O_5	HT	46	0.0	_	_	_	_	_	_
Mo_2C	FD+carb.[d]	38	44.6	63.7	18.3	1.0	0	10.9	6.0
W_2C	FD+carb.[d]	184	44.5	58.1	19.4	1.1	0	17.6	3.9

[a]Mass oxide or mass carbide, corresponding to first column
[b]Conversion and selectivity values are averages of 4 h on stream, namely hours 1-5 for the first MoO_3 entry and hours 21-25 for all other rows
[c]MCH = methylcylcohexane; ECP = ethylcyclopentane; DMCP = dimethylcyclopentane
[d]Carburization of freeze-dried materials in CH_4/H_2 at a final temperature of 650 °C

3.4.2. Toluene vapor phase reaction in H_2 at 350 °C

At 350 °C, induction periods between 6 and 24 h were observed (as exemplified for MoO_3-C in Figure 4); with the starting point defined as the time when a temperature of 350 °C was reached and the end point defined as 90% of the steady state activity. Induction periods decreased in length with increasing surface area of the starting oxide, as a comparison between MoO_3-C and MoO_3-FD revealed, and they increased in length with increasing W/F. Steady state average rates of

toluene conversion were slightly higher for higher initial surface areas; for example, 29 mmol mol_{metal}^{-1} min^{-1} for MoO_3-C vs. 35 mmol mol_{metal}^{-1} min^{-1} for MoO_3-FD. These rates were normalized to moles of metal to eliminate the molecular weight effect for comparison with Mo_2C, which was about an order of magnitude more active under comparable conditions (275 mmol mol_{metal}^{-1} min^{-1}).

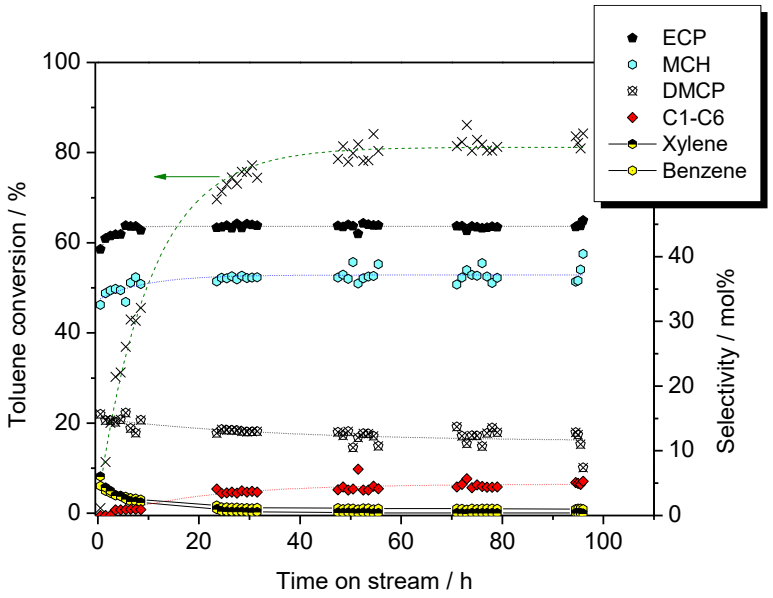

Figure 4: Conversion of toluene vs. time on stream using MoO_3–C as starting material. Reaction conditions: 350 °C, 21 bar, W/F=2.4 h.

Selectivity was largely invariant to time on stream or conversion, with variations not exceeding 5-10 percentage points for any product (Figure 4 and Table 3). Selectivity to the ring hydrogenation product methylcyclohexane (MCH) and the ring contraction products ethylcyclopentane (ECP) and dimethylcyclopentane (DMCP) was exceptionally high, even at high conversions. Selectivity to unwanted short chain alkanes and to benzene and xylene was generally low.

Table 3: Product selectivity for conversion of toluene at 350 °C, 21 bar

Catalyst (Precursor)	W/F (h)	Conv. (%)	Time on stream (h)	Selectivity (C %)						
				C1-C5	C6	MCH	ECP	DMCP	Benzene	Xylene
MoO_3-C	2.4	44	6.5-8.5	0	0.9	36	44	14	2.6	2.1
MoO_3-C	2.4	83	72-100	2.5	2.5	38	45	11	1.0	0.4
MoO_3-C	0.10	15	23-27	0	0	46	30	19	2.5	1.9
MoO_3-FD	0.18	24	21-25	0	0	40	38	17	2.9	1.8
$Mo_{0.86}Nb_{0.14}O_{2.93}$	0.24	18	53-55[a]	0	0	38	38	18	3.1	3.0
Mo_2C	0.04	52	Steady state	10.8	4.7	84.3	1.7	0	0	0

[a]Temperature increased stepwise from 250 to 350 °C over 50 h*

3.4.3. Characterization of MoO_3 before and after 25 h toluene hydrogenation

Post-reaction characterization was performed on several samples of commercial MoO_3 used for 25 h (350 °C, W/F=0.8 h) and showing stable performance (40-55% conversion). The carbon content was determined by the amount of CO_2 formed during TPO. CO_2 evolved between 300 and 500 °C, with a sharp maximum at 400 °C (Figure 5); that is, at temperatures clearly above those for combustion of surface organic matter, consistent with incorporation of carbon. Quantification yielded 0.07 moles of carbon per mole molybdenum, indicating a still predominantly oxidic material.

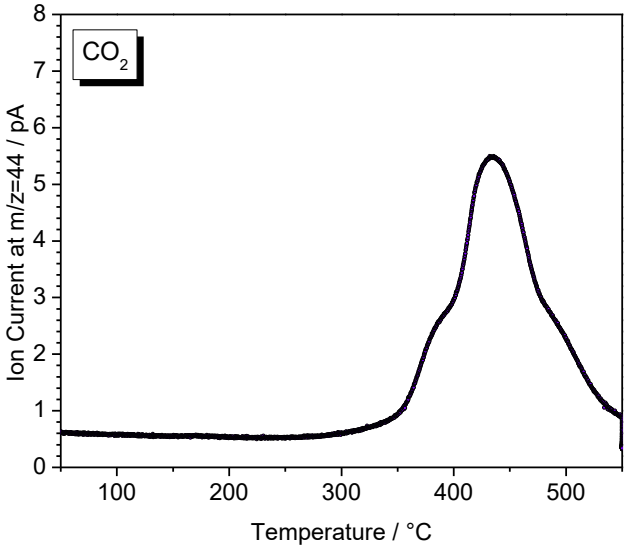

Figure 5: Evolution of CO_2 (m/z=44) during post-reaction temperature-programmed oxidation of catalyst derived from MoO_3. Conditions: 50 ml/min, 20% O_2 in N_2, heating rate 10 °C/min.

Bulk structure analyses of commercial MoO_3 and of the material formed from MoO_3 during toluene conversion at 350 °C are compared in Figure 6. The commercial MoO_3 was orthorhombic and its pattern matched PDF #98-001-4650 (*oP*16, Pbnm). The XRD pattern of the sample exposed to toluene and H_2 for 25 h at 350 °C and subsequently passivated indicated a mixture of phases. One phase was identified as monoclinic MoO_2 structure (*mP*12, P21/c) (Ag_2Te type) (PDF # 01-086-0135). The other phase could not be unambiguously assigned without further analysis, as can be seen by comparison with the patterns of cubic Mo_2C and MoOC.

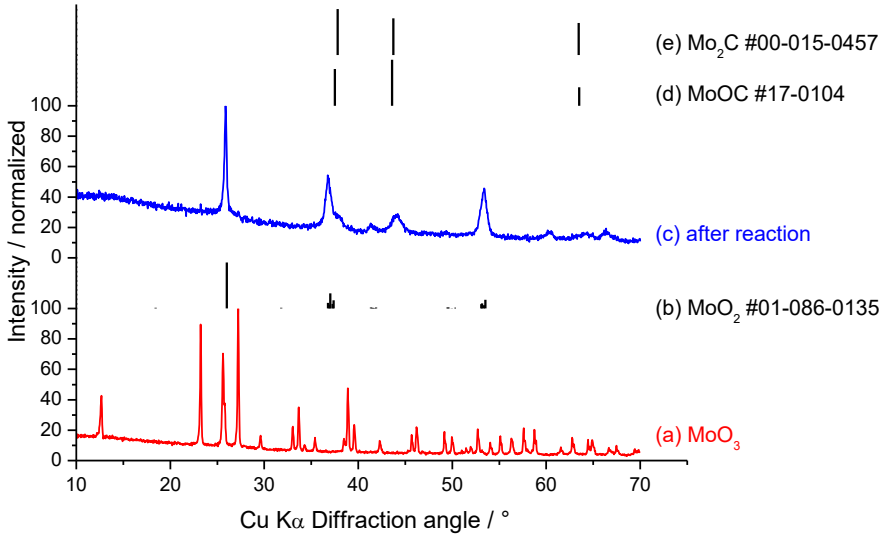

Figure 6: XRD data of MoO_3–C as-received and of the catalyst formed from MoO_3–C at 350 °C through exposure to toluene at 21 bar H_2 for 25 h. (a) MoO_3–C before reaction (fits PDF #98-001-4650), (b) MoO_2 PDF #01-086-0135, (c) catalyst after reaction, (d) MoOC PDF #17-0104, and (e) Mo_2C PDF #00-15-0457.

To interpret the diffractogram of the material removed from the reactor after 25 h operation at 350 °C, the pattern of the MoO_3 used as starting material (PDF# 00-005-0508, *oP*16),[38] was analyzed first. It could be fit without application of a preferred orientation and with a FWHM of 0.12 degrees 2Θ. The pattern of the phase mixture formed in the feed was well described by a combination of monoclinic MoO_2 and a cubic structure. The monoclinic MoO_2 peaks were fit with a FWHM of 0.30 degrees, consistent with crystallite domain sizes of about 46 nm. The cubic structure with the stoichiometry of Mo_2C (PDF#015-0457) did not give a good fit for the intensity ratio of the (111) and (200) reflections in the material recovered from the reactor (Figure 7), and the determined unit cell length of 4.10 Å is significantly shorter than the 4.155 Å reported on card #00-015-0457. The cubic structure was fit with a FWHM of about 1.3 degrees, consistent with domain sizes of about 8 nm.

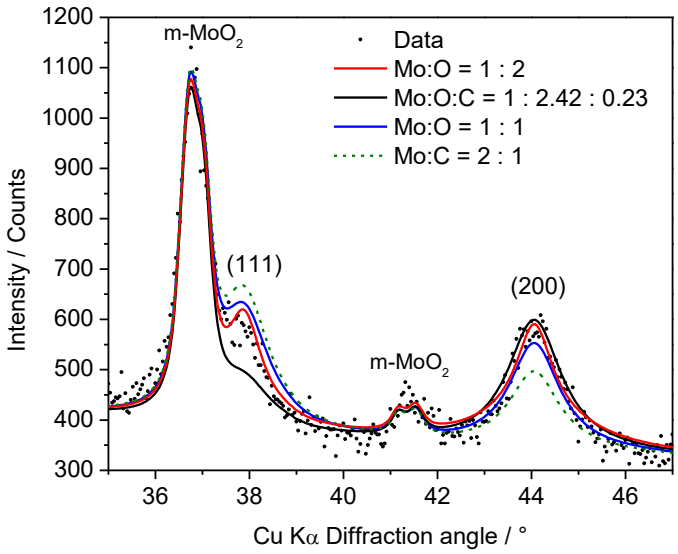

Figure 7: Detail of fits of the XRD pattern of material retrieved from the reactor after exposing MoO_3 to toluene/H_2 for 25 h and passivation in air. Fits include monoclinic MoO_2 (PDF #01-086-0135) and a cubic phase with various stoichiometries as indicated. Reflections of cubic phase are indexed.

Table 4 gives on overview of reported phases and the characteristics of their diffractograms in comparison with the cubic phase recovered from the reactor. A cubic structure formed through the reduction of MoO_3 and with a lattice constant of 4.10 Å was previously reported by Bouchy et al.[23] and identified as $MoO_{2.42}C_{0.23}H_{0.78}$. Alternatively, a cubic structure has also been identified as a MoO species.[39] The intensity ratios in the pattern of the recovered material could better be matched with a stoichiometry of 1 or 2 oxygens per molybdenum (Figure 7) than with that reported by Bouchy. However, TPO indicated the presence of carbon, and the lattice constant matched that reported by Bouchy et al. (see Table 4). From the XRD data, the monoclinic MoO_2 phase constitutes about 43 wt% of the sample and the cubic phase constitutes about 57 wt% of the sample (for Mo:O = 1:2 stoichiometry of the cubic phase with half of the metal sites vacant).

Table 4: Observed diffraction parameters and previously reported diffraction parameters for cubic molybdenum oxides, oxycarbides and carbides

Material	Source	Lattice constant, (Å)	Reflections by *hkl* (Relative Intensity)			
			1 1 1	2 0 0	2 2 0	3 1 1
MoO	Torres et al.[39]	4.08	38.337	44.370	64.678	n.r.
MoOC	Bouchy et al.[23]	4.10	38.000 (27)	44.210 (100)	64.228 (27)	
MoOC	Ferguson et al. [40]	4.15-4.18	37.496 (m)	43.581 (m+)	63.474 (w)	76.054 (w+)
MoOC	PDF 17-0104	4.152	37.506 (80)	43.582 (100)	63.491 (40)	76.082 (50)
Mo_2C	PDF 015-0457	4.155	37.800 (100)	43.731 (80)	63.453 (70)	75.799 (70)
α-MoC	Frauwallner et al.[24]		36.8	43.9	62.9	
Ex reactor 25 h	Observed	4.10	38.00 (100)	44.16 (94)	64.23 (57)	

Scanning electron microscopy was used to track any major changes in particle morphology during the catalytic reaction and also during subsequent temperature-programmed oxidation. The starting MoO_3 (Figure 8a and b) consisted of large particles, reaching 50 μm in the longest dimension, which, typical of an insulator, were prone to charging. These particles had typical traits of single crystals such as straight edges at well-defined angles. The crystals were characterized by two distinctly different types of surface that were found to be perpendicular to each other. The appearance is consistent with the layered structure of orthorhombic MoO_3; and smooth surfaces are presumably parallel to the sheets, whereas the stepped surfaces arise from the edges of sheets.

After 25 h of reaction in toluene and H_2, the particle size was reduced, the smooth, flat surfaces were disrupted, and the particles presented cracked and corrugated surfaces decorated with smaller particles (Figure 8c). Close inspection showed a substructure with regular, elongated smaller features on the order of ≈50 nm. In the "side view", the previously layered appearance with long facets were replaced by rough edges (Figure 8d). The layered structure was clearly broken up,

presenting deep crevices and gaps between the layers. The particles showed much less tendency to charge after reduction.

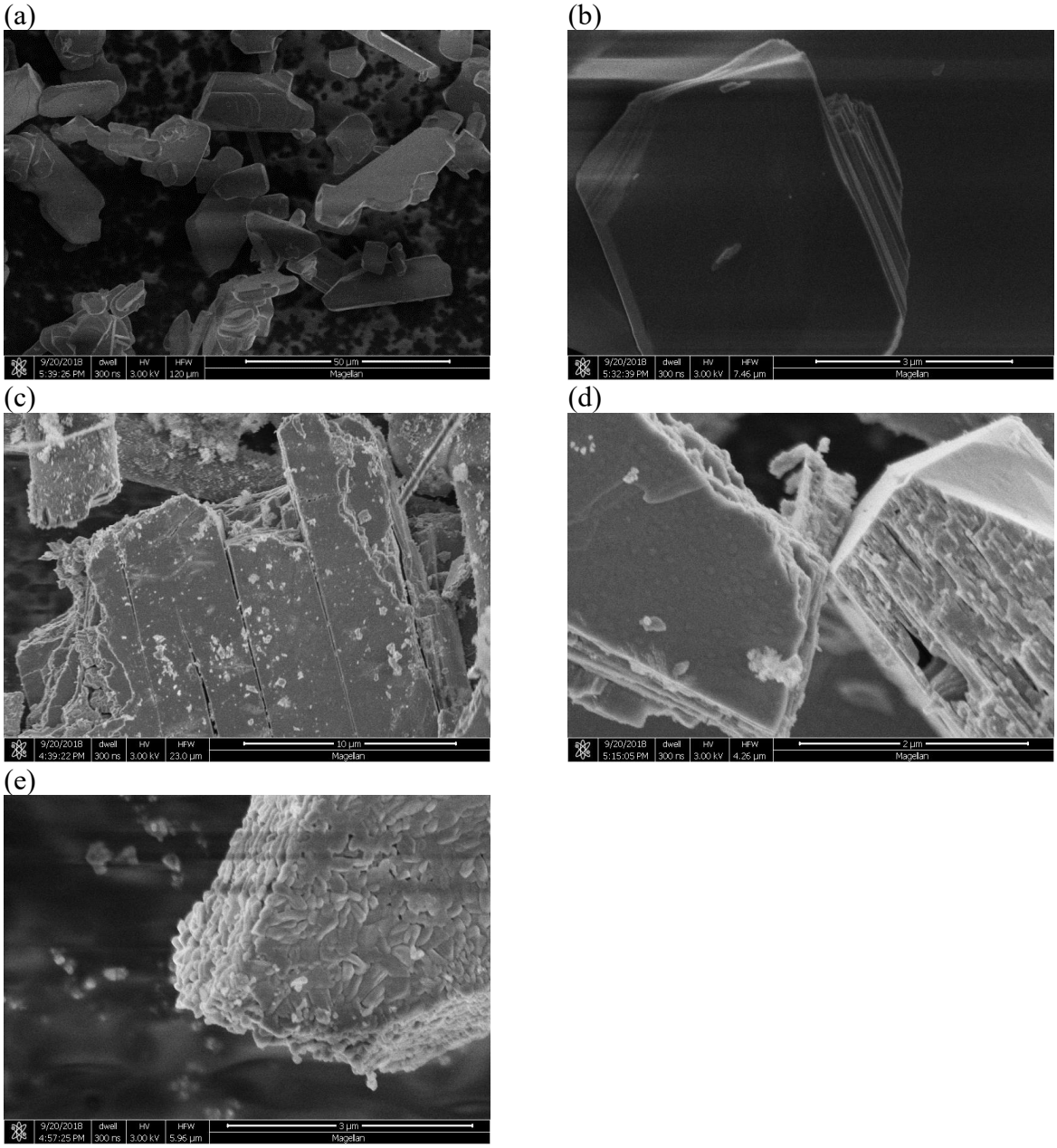

Figure 8: Scanning electron micrographs of starting MoO_3 (a,b), a material removed from the reactor after 25 h of operation at 21 bar H_2/toluene and a temperature of 350 °C (c,d) and a material that was additional heated at 10 °C /min in 20% O_2 up to a temperature of 550 °C.

This change in morphology was not reversed by re-oxidation of the material at a temperature of 550 °C. The particle size was retained, but aggregates of small, relatively uniform grains were formed rather than single crystals (Figure 8e). The grains were short needles with rounded edges or corners. In the side view, the layered structure was still recognizable but had lost the edginess of the active material.

The N_2 adsorption isotherms of MoO_3 before reaction and of its products obtained after reaction in toluene and H_2 (and passivation) are compared in Figure 9. The results show that the as-received MoO_3 had a very low surface area (0.3 m^2/g) and no detectable porosity, whereas the material removed from the reactor had a surface area of 20 m^2/g and micro- as well as mesopores. The BJH desorption pore volume and average pore size were determined to be 0.018 $cm^3\ g^{-1}$ and 4.8 nm, respectively.

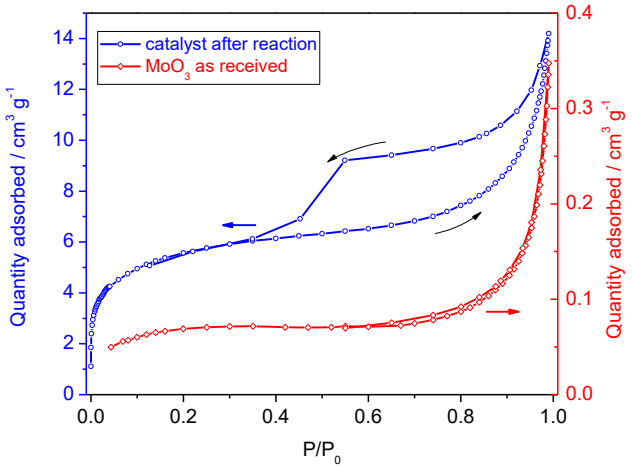

Figure 9: N_2 adsorption isotherms of MoO_3–C as-received and of the catalyst formed from MoO_3–C during toluene hydrogenation. (Reaction conditions: 350 °C, 21 bar H_2 and toluene, W/F=0.8 h, 25 h on stream, passivated).

The surface sites of the active catalyst samples were characterized in situ, by adsorbing bases after purging the reactor with inert gas and cooling to an appropriate temperature. Several probes with different proton affinities were used, namely isopropylamine: 912 kJ/mol; acetonitrile: 779 kJ/mol; and 2,6-dimethylpyridine (2,6-lutidine): 955 kJ/mol.[41,42] The adsorbed amounts of

isopropylamine and acetonitrile consistently indicated about 0.4 mmol acid sites per g MoO_3. The formation of propylene from isopropylamine[43] upon heating proved the presence of Brønsted acid sites (Figure 10a). Secondary reactions of propene seen in concomitantly recorded gas chromatograms prohibited quantification of the Brønsted sites from this MS trace. TPD of acetonitrile revealed at least three different types of acid sites that varied significantly in strength (Figure 10b). The adsorbed amount of lutidine was less than that of the other bases at about 0.26 mmol/g MoO_3.

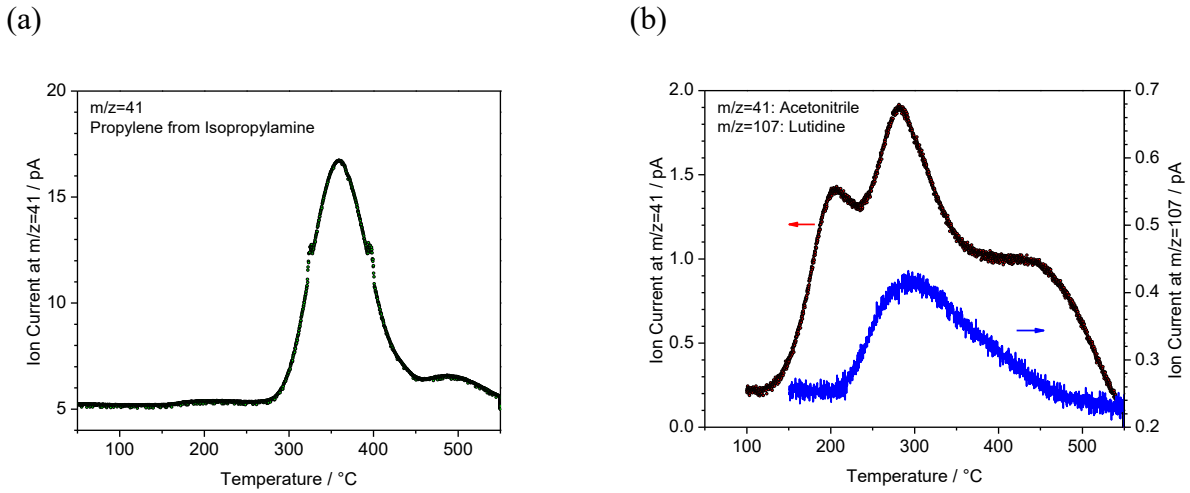

Figure 10: Mass spectra recorded during heating of a MoO_3-derived active catalyst after adsorption of (a) isopropylamine and (b) acetonitrile or lutidine. Catalyst created over 25 h at 350 °C and 21 bar H_2/toluene, purged, exposed to base and then heated in 50 ml/min N_2 flow at a heating rate of 10 °C/min.

4. Discussion

4.1. Properties, reduction and carburization of pure oxides and mixes oxides

The pure oxides prepared via the freeze-drying method were characterized by much higher surface areas than commercially acquired MoO_3 and WO_3 materials (Table 1), which explains why their reduction starts and progresses further at lower temperatures. Prior literature[30] reports that oxygen vacancies form more easily in smaller particles because more Mo=O bonds are exposed,

and this effect could be pronounced since the FD-MoO_3 particles are more than one order of magnitude smaller than those in the cited paper. For commercially acquired, coarse-crystalline oxides, individual reduction steps are not necessarily discernable, but MoO_3 and WO_3 are both known to be first reduced to MoO_2 and WO_2, respectively.[44,45] Here, the FD-prepared WO_3, which has an estimated particle size of 110 nm (from surface area assuming spheres), was reduced more significantly in the first step and passes through a metallic phase before forming a carbide.[46]

The presence of niobium in the oxides increased their surface area relative to pure MoO_3 as indirectly observed before when analyzing carbides produced from such mixed oxides.[37] The high surface areas of the hydrothermally prepared oxides are thus more likely associated with the high niobium content than with the preparation methods. The high surface areas may in part explain why the mixed oxides reduce at lower temperature than the pure oxides. In addition, it has been proposed that substitution of Mo^{6+} by Nb^{5+} generates oxygen vacancies to maintain charge balance, and vacancies are known to facilitate bulk diffusion.[37] For mixed Mo-W-oxide, the same argument cannot be used as both metals have the valence +VI. A possibility is that the mixed oxide is more defective, which may enhance bulk diffusion.

CO formation began at temperatures between 570 and 645 °C and occurred generally in parallel with water formation (Figure 1), but only after the sample was substantially reduced with about 2/3 of the oxygen removed. This observation suggests that for methane activation (and carbide formation), the surface needs to be near-metallic. Since transport of oxygen from the bulk will be rate-limiting, the surface may in fact be more reduced than the stoichiometry (by TG) suggests. The pure oxides were largely reduced by H_2, whereas the mixed oxides released some oxygen as CO. Apparently, not enough activated hydrogen is available to react with emerging oxygen (or formed CO) to prevent release of CO. It follows that the surfaces of the ternary compounds are

less active for H_2 activation than those of the binary compounds, which is consistent with lower selectivity toward C1-C6 alkanes (Table 2).

4.2. Reduction of oxides at high pressure H_2/toluene

During exposure to toluene, three parameters differed in comparison to the carburization in methane: the H_2 pressure, the nature of the hydrocarbon, and the final temperature. H_2 pressure influences the H_2 coverage on the surface, which affects the rate of H_2 activation, and, through the gradient, also the rate of diffusion into the bulk. It is conceivable that H diffuses into the bulk since these oxides are known to form bronzes. It is also known that longer hydrocarbons are more reactive and lead to lower carburization temperatures.[47] Finally, the temperature affects diffusion of species out of and into the bulk.

The reduction through H_2 at 21 bar occurred at lower temperature than at atmospheric pressure. The maxima of H_2O evolution shifted from 450 °C to 325 °C ($Mo_{0.86}Nb_{0.14}O_{2.93}$), 500 °C to 375 °C ($Mo_{0.5}W_{0.5}O_3$) and 575 °C to 375 °C ($MoO_3$). The shift is consistent with prior observation of removal of passivation layers at lower temperature when the H_2 pressure was raised.[13] The reduction sequence seen among the materials in H_2/CH_4 at atmospheric pressure was preserved in H_2/toluene; thus the arguments made earlier regarding the influence of surface area and oxygen vacancies formed through substitution with a lower valent cation have general validity.

At a final temperature of 400 °C, the normalized water peaks for all molybdenum-containing samples were equal, implying the same degree of reduction and a defined bulk stoichiometry. The data in Figure 1 indicated that one oxygen per metal is easily removed from these oxides, resulting in a MeO_2 stoichiometry. At 350 °C, MoO_3-FD reached 80% of the degree of reduction that was reached at 400 °C, suggesting an incomplete reduction step with possible approach to MeO_2

stoichiometry. Reduction to a stoichiometry of 2 oxygens per molybdenum is also supported by the XRD analysis of the material from the reactor after 25 h at 350 °C (Figure 7).

The H_2O peak areas seen for WO_3 during activation at 400 °C and for MoO_3-C at 350 °C are clearly below the expectation for removal of 1 oxygen per metal, suggesting that only the surface is reduced during the first 100 min. Long tails of the water peaks indicated continued reduction. Materials that did not complete the reduction step to MeO_2 during the first 100 min (consisting of the heating ramp and a short hold) exhibited induction periods of several hours, consistent with slow equilibration in the feed stream associated with change of the composition.

4.3. Catalytic performance in toluene conversion and nature of active surface

4.3.1. Reported phases in H_2/hydrocarbon atmospheres, associated sites and introduction to toluene reaction pathways

There is dissent in the literature as to the origin of catalytic activity when exposing oxides such as MoO_3 to a hydrocarbon/H_2 feed. The Mo-O-C-H phase chemistry is rich in polymorphs and sub-stoichiometric phases. As the literature data in Table 5 show, bronzes (H-containing materials) may be formed in the absence of carbon-containing molecules. In the presence of H_2 without a carbon source, formation of MoO_2,[34] reduced MoO_3,[35] molybdenum oxyhydride MoO_xH_y,[36,48] and partially reduced MoO_3 with Brønsted acid groups $MoO_3(H_x)_{ac}$ have been reported.[49] At high temperatures, carbides are formed. At 400 °C and 0.6 bar toluene and with MoO_3 as starting compound, formation of MoO_2, MoO_xC_y and a surface or bulk carbide would be expected.[23,24,26] The ambiguity arises at temperature of 350 to 370 °C. MoO_2, MoO_xC_y, and MoO all have been reported under conditions similar to those applied here, except that alkanes or 4-methylphenol were applied and not toluene (see Table 5). The structures are not easily distinguishable, as can be seen from Table 4. At 350 °C, surface carbide formation has been claimed to be insignificant.[26]

The product distribution of toluene conversion is diagnostic of the sites present on the catalyst surface. Ring hydrogenation requires a metal site that activates H_2. Ring contraction is an isomerization and can be catalyzed by an acid, with stronger acids leading to di-substituted rings.[50] Alternatively, the contraction can be catalyzed by a metal, for example platinum.[51] Toluene disproportionation requires strong acid sites such as those of HZSM-5;[52] toluene hydrodealkylation can occur on metallic sites.[53] Short-chain alkanes may be formed by hydrogenolysis on a metal,[54] whereby the product distribution depends on the properties of the metal. For example, palladium and rhodium preferentially cleave the terminal C-C bond in a chain, giving methane and a C_{n-1} alkane, whereas platinum and iridium give a close-to-statistical cleavage pattern. Nickel leads to successive demethylation. Small alkanes may also be formed by acid-catalyzed cracking and subsequent hydrogenation, with the possibilities of Haag-Dessau cracking or beta scission. The former leads to a statistical product distribution of alkanes, whereas the latter will preferentially cleave a C7 hydrocarbon into C3 and C4 hydrocarbons.

4.3.2. Surface site evolution during toluene conversion at a temperature of 400 °C

When a temperature of 400 °C was reached, all samples hydrogenated toluene to methylcyclohexane, indicating the presence of metallic surface sites capable of H_2 activation and ring hydrogenation. The high rates and high selectivities to short alkanes (from hydrogenolysis) typical of carbidic surfaces were not observed at this time on stream, suggesting a different type of surface. The degree of reduction at the end of the ramp corresponds to MeO_2 stoichiometry for all molybdenum-containing samples, and the slow increase in rate for WO_3 (Figure 3) is consistent with its somewhat slower reduction. Both MoO_2 and WO_2 are known to exhibit metallic properties.[55] The formation of MoO_2 from MoO_3 was observed under similar conditions by Frauwallner et al.[24] and Vitale et al.,[25] who treated MoO_3 in toluene/H_2 at 400 °C; however, they

claimed that bulk fcc α-MoC (PDF# 015-0457) formed in addition to MoO_2. Torres et al.,[39] after subjecting MoO_3 to a H_2/*n*-heptane mixture at 18.5 bar and 370 °C, identified a metallic MoO phase, but the MS data in Figure 2 do not support this stoichiometry in the present case. The data here suggest that the initial reactivity of the surface is attributable to metallic oxides MeO_2.

There were three indications that acidic sites are temporarily present during the early phase on stream on the molybdenum-containing samples; these are ring contraction (i.e., skeletal isomerization) products with ethylcyclopentane predominating over dimethylcyclopentane, disproportionation products benzene and xylene, and C3 and C4 alkanes, which indicate beta scission rather than alkanium ion cracking. The results are consistent with earlier reports of ring contraction of methylcyclohexane on partially reduced MoO_3 "$MoO_2(H_x)_{ac}$" at 300 °C [49] and on partially reduced WO_3 "$WO_2(H_x)_{ac}$" at 400 °C.[56] Both, the prevalence of the mono- over the disubstituted ring contraction product and the beta scission over protolytic cracking indicate Brønsted acid sites of medium and not of high strength. Disproportionation, however, is reported to require a strong acid.[52]

Over time on stream at 400 °C, MoO_3 and WO_3 transformed into more active materials, and the selectivity shifted towards hydrogenolysis to small alkanes. Thus, they more and more resembled the carbides Mo_2C and W_2C, which are highly active and mainly produce short alkanes at 400 °C (Table 2), in particular methane. Consistent with this observation, the opposite trend was observed by Choi et al. when Mo_2C was exposed to increasing amounts of oxygen;[12] namely, the benzene hydrogenation ability was inhibited. The transition to carbide happened more quickly for MoO_3, which is known to carburize at lower temperatures than WO_3 (Figure 1). WO_3 also became more active, but the increase in cyclopentanes and in short alkanes occurred in parallel; however, at 25 h, hydrogenolysis products already constitute the largest fraction. The evolution with time is

consistent with observations by Blekkan et al.[16] during *n*-heptane conversion with MoO_3 as starting material, who also detected C3 and C4 alkanes at short times on stream and more C1 and C6 alkanes at longer times on stream. On the basis of the reports by Frauwallner et al.[24] and Vitale et al.[25] and those of Delporte et al.[26] and Bouchy et al.,[23] the formation of a carbidic phase or at least surface layer from MoO_3 is expected at 400 °C. Hence, at longer times on stream, carbides or at least surface carbides form from the MoO_3 and WO_3 starting materials.

The effect of the second metal is threefold: The reduction is more facile, resulting in a faster approach to steady state; carbide formation is suppressed, resulting in stable performance and less hydrogenolysis. Also, the highest concentrations of C3 and C4 alkanes are observed for the mixed Mo-Nb and Mo-W materials, indicating that addition of a second metal enhances the Brønsted-acidity of these materials.

4.3.3. Nature of material recovered after operation at 350 °C

XRD and TPO shows that material removed from the reactor after operation at 350 °C is largely oxidic and not carbidic. Two phases were identified, monoclinic MoO_2 and a cubic phase $Mo_{1-x}O$ with $x \approx 0.5$. This steady-state chemical composition is consistent with the achievable degree of reduction estimated on the basis of the water peaks in Figure 2, with reduction being incomplete during the heating ramp. Even if it is assumed that the carbon is solely associated with the cubic phase, the molybdenum-to-carbon ratio in this phase is only 1.0:0.12. The carbon content is lower than specified by Bouchy et al. (Mo:C=1.0:0.23) or Ferguson et al. (Mo:C = 1.0:0.31±3) for the reported oxycarbides. Given that also the relative reflection intensities could be fit better with carbon-free stoichiometries, the phase is probably not a bulk carbide.

The surface area, which increases from 0.3 m^2/g to 20 m^2/g (Figure 8), and the size of the crystalline domains as determined by XRD are principally consistent. Assuming spherical particles

and a density range between that of MoO_2 and Mo_2C, the surface area translates to particle diameters of 13-18 nm, between the domains sizes of 46 nm for MoO_2 and 8 nm for the cubic phase. Given that coarse-crystalline MoO_3 is the starting material, the domains of MoO_2 are probably retained crystallites of the original MoO_3. In contrast, the second phase is probably a newly nucleated phase, with slowly growing domains. The increase of surface area during reduction of oxides or carburization is a well-known phenomenon[57] that some authors have associated with bronze formation.[36,58] A simple explanation is the higher density of MoO_2 and the cubic Mo-O-C phase relative to that of MoO_3 (6.46 g/cm^3 and 6.17 g/cm^3 vs. 4.71 g/cm^3), which implies shrinkage of the volume and associated fissure formation. This latter hypothesis is corroborated by the SEM images that show shrunk sections surrounded by gaps and a general break-up of the layered structure.

The surface was found to be characterized by a total amount of about 0.4 mmol/g acid sites, which translates to a dense population considering the surface area of 20 m^2/g. Per mole molybdenum, there are more acid sites than there is carbon, underlining the oxidic character that produces both Brønsted and Lewis acid sites. Formation of propylene from isopropylamine proves the presence of Brønsted acid sites. Lutidine selectively adsorbed on a subgroup of only 0.26 mmol/g sites in comparison to the other, weaker bases. Lutidine has been used to preferentially probe Brønsted over Lewis sites.[59] While this claim has been debated,[60] no lutidine desorbed below 200 °C during TPD, implying that only Brønsted and very strong Lewis acid sites were probed.[60] Combining these results with the profile observed in the acetonitrile TPD, the weak acid sites are probably Lewis acid sites, commensurate with reduced and thus soft coordinatively unsaturated molybdenum ions. The highest temperature m/z peak in the acetonitrile trace is somewhat questionable since hydration of acetonitrile was observed concomitantly. The maximum in the

acetonitrile curve and the moderate temperature for desorption of most of the lutidine suggest that the predominant type of site is a medium-strength Brønsted acid.

4.3.4. Surface-site evolution for MoO_3-derived material at 350 °C

When a reaction temperature of 350 °C was reached, the MoO_3-derived materials briefly produced a higher fraction of disproportionation products, which can be explained with temporarily present strong Brønsted acid sites, as also seen at 400 °C. Generally, the acid strength of oxo-anion acids is higher with higher number of oxygens, which is equivalent to a higher oxidation state of the central atom, and hence observation of beta scission and toluene disproportionation would be expected early on stream when the samples are less reduced.

At steady state, ring hydrogenation and ring contraction products indicate the presence of both metallic and acidic sites. Metallic sites are likely provided by MoO_2. There are only isolated observations of aromatic ring hydrogenation by this type of catalyst.[61] These metallic sites are unique, since they do not catalyze hydrogenolysis. While the sample does contain carbon, the concentration may be too low to provide ensemble sites needed for hydrogenolysis, or the surface does not provide enough atomic hydrogen. The inability of the surface to catalyze hydrogenolysis may self-protect it from carbide formation, which would require the formation individual C atoms. In contrast to operation at 400 °C, the surface did not transition to carbidic behavior. Dealkylation of toluene to benzene and a C1 fragment may be another route to carbide formation. In this case, tungsten would not be a good additive because it was reported to promote dealkylation, at least at a temperature of 400 °C.[46]

Comparison with equilibrium mole fractions shows that the product distribution was determined by kinetics and not thermodynamics, which would favor both methylcyclohexane and dimethylcyclopentanes significantly over ethylcyclopentane. This result is consistent with the

probe molecule results, the majority of sites are of medium strength and can catalyze the ring contraction, whereas strong acid sites for branching isomerization to the dimethylcylcopentanes are not available.

The role of carbon is ambiguous in the literature. There are two hypotheses for the active phase: materials containing no or inactive carbon,[62] as opposed to oxycarbides. Materials in the first group are of the general composition MoO_xH_y and include MoO_2, which has been proposed to be the active phase[34] and also has been dismissed as active phase in skeletal alkane isomerization.[64] Alternatively, MoO_x with a stoichiometry close to MoO and containing much hydrogen was considered to be the active phase in hexane isomerization.[64] Similarly, "reduced MoO_3" was proposed to isomerize *n*-heptane via a bifunctional mechanism on Brønsted acid sites and Mo metal sites.[35,63] This conclusion was supported by similar product distributions as observed with Pt/USY, which consisted of 2- and 3-methylhexane and, at higher conversions, of increasing amounts of dimethylpentane. A bifunctional mechanism was also inferred by Belatel et al.,[49] who considered a surface $MoO_{2x}(H_x)_{ac}$ phase as active phase. Methylcyclohexane was isomerized to ethylcyclopentane and dimethylcyclopentane, and at 380 °C, was dehydrogenated to toluene. In sum, these phases exhibit a mixture of Brønsted and metallic sites and the associated bifunctional reaction characteristics, which include, general similarity of the product distribution to classical bifunctional catalysts such as Pt/zeolites, central cleavage of hydrocarbons (e.g., C3+C4 from C7), selectivity a function of conversion with increase in branching, cyclization, and dehydrogenation.

In contrast, MoO_xC_y was reported to produce mainly monobranched isomers during heptane isomerization, selectivity was not a function of conversion, and if cleavage was seen, then mainly demethylation. This pattern was explained with a single site and a metallacycle bond shift mechanism.[16]

As Table 3 shows, there are almost no cleavage products, and if they are formed, then mainly C6, suggesting demethylation, rather than cleavage into C3 and C4. The product distribution also was not a function of conversion over a wide range of conversions (except for the first 1-2 h at reaction temperature). These results suggest that the active phase is closer in nature to those observed by Blekkan et al.[16] and Bouchy et al.[29] than to the MoO_xH_y phases described by Matsuda et al.,[35,63] Wehrer et al.,[64] and Belatel et al.[49] . Given the small concentration of carbon, also relative to the concentration of acid sites, carbon may not play a role as part of an active site. It also not necessary to infer a role, since another metallic phase is present, MoO_2, and the acid sites are clearly associated with oxygen.

The reasons for the formation of the different phases reported in the literature and their associated catalytic behavior also become apparent. The bifunctional catalysts formed under atmospheric pressure conditions with low hydrocarbon partial pressure (or pulses), whereas the oxycarbides and the phases displaying similar behavior are formed at elevated H_2 and hydrocarbon partial pressure. The effect of pressure was also reported by Del Gallo et al.[66] Higher temperatures also promote carbide formation as is obvious from Table 5.

.

Table 5: Observed phases and trends in molybdenum compound reduction and carburization.

Starting Material	Temp. / °C	Atmosphere	Phases	Comments	Refs.
MoO_3	350	H_2, up to 1 atm	Bronze H_xMoO_3, hydride MoO_xH_y, MoO_2, Mo metal (in this sequence over time)	- High H_2 partial pressure (1 atm) and low temp. (350 °C) favor MoO - Water vapor inhibits further reduction of MoO_2 (and oxycarbides) to Mo metal	Matsuda et al.[35]; Wehrer et al. [64,65]
MoO_3	350	H_2/toluene=35 at 21 bar	MoO_2 (*mP*12, P21/c) and cubic MoO_x		This work
MoO_3	350	H_2/4-methylphenol at 44 bar	MoO_2 and maybe Mo_4O_{11}		Whitten and Smith[61]
Orthorhombic MoO_3	350	H_2/*n*-butane or H_2/*n*-heptane) from 2 to 150 at 1 to 40 atm	Sub-oxide MoO_2 and an oxycarbide phase, MoO_xC_y	- High pressure promotes formation of oxycarbide	Bouchy et al.[20,23]; Del Gallo et al. [66]
Molybdenum bronze $H_{0.34}MoO_3$	350	H_2/*n*-heptane=30 at 7 bar	Pure oxycarbide phase, MoO_xC_y	- Bronze formation is necessary for oxycarbide synthesis	Bouchy et al. [29]
MoO_3	370	H_2/*n*-heptane=39 at 18.5 bar	Metallic-like MoO in MoO_x matrix	- MoO better match for XRD and HRTEM than MoOC	Torres et al.[39]
MoO_3	400	H_2/toluene at 60 bar	Mo_2C (*cF*6, Fm-3m) NaCl type and MoO_2 (JCPDS01-076-1807)		Frauwallner[24]
Various oxidized forms of Mo	650 (ramp)	H_2/CH_4=9; hexane, toluene <0.01 vol.%, in H_2	Hexagonal Mo_2C (methane) or cubic MoC_{1-x} (hexane and toluene)	- No oxycarbide phase observed as intermediate - Carbide formation at 550 °C possible under isothermal conditions and with long reaction times	Guzman et al.[67]

5. Conclusions

Non-noble metal catalysts capable of aromatic ring hydrogenation and skeletal isomerization were obtained by treating MoO_3 or WO_3, or mixed oxides of molybdenum with tungsten or niobium in a feed of toluene and H_2 at 350 °C or 400 °C and 21 bar. At 400 °C, increasing selectivity to short-chain alkanes indicated slow carbidization of the materials over time. At 350 °C, carbidization was suppressed, and high selectivity to ring contraction products (≥50%) combined with low selectivity towards C-C bond cleavage products (≤5%) was obtained when starting with MoO_3. The catalyst was stable over 95 h on stream.

In situ TPR data and the XRD pattern of the active MoO_3-derived catalyst retrieved from the reactor after operation at 350 °C indicated an overall Mo:O stoichiometry of 1:2 and two phases, monoclinic MoO_2 and cubic $Mo_{1-x}O$. While incorporation of carbon into the cubic phase could not be excluded, the best fit of the diffractograms was obtained without carbon. Similar phases reported before are known to catalyze alkane isomerization; however, the ability of this catalyst to hydrogenate aromatic rings underscores the metallic properties, while the selectivity to ring contraction is exceptional.

The presence of a second metal cation, specifically niobium or tungsten, facilitated reduction of the oxide bulk, and steady state was reached more quickly. A second advantage is that both niobium and tungsten oxides are more difficult to carburize than molybdenum and can prevent carbide formation. Hence, mixed oxides, particularly with infinitely adaptive structures, present excellent prospects for optimization of this type of catalyst.

6. Acknowledgments

Acknowledgment is made to the Donors of the American Chemical Society Petroleum Research Fund for support (or partial support) of this research under PRF#51448-ND5. This work

was, in part, supported by National Science Foundation award 0923247 (thermal analysis equipment as part of a major research instrumentation grant). This work was supported by the United States Department of Energy under Grant No. DE-SC0004600. The authors thank Lance L. Lobban for providing a test reactor and Sanket Sabnis for help with SEM.

7. References

[1] H. Du, C. Fairbridge, H. Yang and Z. Ring, The chemistry of selective ring-opening catalysts, *Appl. Catal., A*, 2005, **294**, 1–21.

[2] A. Martínez, M. A. Arribas and S. B. C. Pergher, Bifunctional noble metal/zeolite catalysts for upgrading low-quality diesel fractions via selective opening of naphthenic rings, *Catal. Sci. Technol.*, 2016, **6**, 2528-2542.

[3] G. B. McVicker, M. Daage, M. S. Touvelle, C. W. Hudson, D. P. Klein, W. C. Baird, Jr., B. R. Cook, J. G. Chen, S. Hantzer, D. E.W. Vaughan, E. S. Ellis and O. C. Feeley, Selective ring opening of naphthenic molecules, *J. Catal.,* 2002, **210**, 137–148.

[4] D. Santi, T. Holl, V. Calemmab, J. Weitkamp, High-performance ring-opening catalysts based on iridium-containing zeolite Beta in the hydroconversion of decalin, *Appl. Catal., A* 2013, **455,** 46– 57.

[5] J. H. Sinfelt and D. J. C. Yates, Effect of carbiding on hydrogenolysis activity of molybdenum, *Nature (London), Phys. Sci.*, 1971, **229**, 27.

[6] R. B. Levy and M. Boudart, Platinum-like behavior of tungsten carbide in surface catalysis, *Science*, 1973, **181**, 547-549.

[7] J. R. Kitchin, J. K. Nørskov, M. A. Barteau and J. G. Chen, Trends in the chemical properties of early transition metal carbide surfaces: A density functional study, *Catal. Today*, 2005, **105**, 66-73.

[8] A. J. Medford, A. Vojvodic, F. Studt, F. Abild-Pedersen and J. K. Nørskov, Elementary steps of syngas reactions on Mo_2C (001): Adsorption thermochemistry and bond dissociation, *J. Catal.*, 2012, **290**, 108-117.

[9] F. H. Ribeiro, M. Boudart, R. A. Dalla Betta and E. Iglesia, Catalytic reactions of *n*-Alkanes on β-W_2C and WC: The effect of surface oxygen on reaction pathways, *J. Catal.*, 1991, **130**, 498-513.

[10] E. Iglesia, J. E. Baumgartner, F. H. Ribeiro and M. Boudart, Bifunctional reactions of alkanes on tungsten carbides modified by chemisorbed oxygen, *J. Catal*., 1991, **131**, 523-544.

[11] E. Iglesia, F. H. Ribeiro, M. Boudart and J. E. Baumgartner, Synthesis, characterization, and catalytic properties of clean and oxygen-modified tungsten carbides, *Catal. Today*, 1992, **15**, 307-337.

[12] J.-S. Choi, G. Bugli and G. Djéga-Mariadassou, Influence of the degree of carburization on the density of sites and hydrogenating activity of molybdenum carbides, *J. Catal.*, 2000, **193**, 238-247.

[13] A. Mehdad, R. E. Jentoft, F. C. Jentoft, Passivation agents and conditions for Mo_2C and W_2C: Effect on catalytic activity for toluene hydrogenation *J. Catal.*, 2017, **347**, 89–101.

[14] F. H. Ribeiro, R. A. Dalla Betta, M. Boudart, J. Baumgartner and E. Iglesia, Reactions of neopentane, methylcyclohexane, and 3,3-dimethylpentane on tungsten carbides: The effect of surface oxygen on reaction pathways, *J. Catal.*, 1991, **130**, 86-105.

[15] M. M. Sullivan, J. T. Held and A. Bhan, Structure and site evolution of molybdenum carbide catalysts upon exposure to oxygen, *J. Catal.*, 2015, **326**, 82-91.

[16] E. A. Blekkan, C. Pham-Huu, M. J. Ledoux and J. Guille, Isomerization of *n*-heptane on an oxygen-modified molybdenum carbide catalyst, *Ind. Eng. Chem. Res.*, 1994, **33**, 1657-1664.

[17] S. J. Ardakani, X. Liu and K. J. Smith, Hydrogenation and ring opening of naphthalene on bulk and supported Mo_2C catalysts, *Appl. Catal. A*, 2007, **324**, 9-19.

[18] M. M. Sullivan and A. Bhan, Acid site densities and reactivity of oxygen-modified transition metal carbide catalysts, *J. Catal.*, 2016, **344**, 53-58.

[19] W. -S. Lee, A. Kumar, Z. Wang and A. Bhan, Chemical titration and transient kinetic studies of site requirements in Mo_2C-catalyzed vapor phase anisole hydrodeoxygenation, *ACS Catal.*, 2015, **5**, 4104-4114.

[20] C. Bouchy, C. Pham-Huu, B. Heinrich, E. G. Derouane, S. B. Derouane-Abd Hamid and M. J. Ledoux, In situ TPO, TPD and XRD characterisation of a molybdenum oxycarbohydride catalyst for *n*-butane isomerisation, *Appl. Catal. A*, 2001, **215**, 175-184.

[21] P. Delporte, F. Meunier, C. Pham-Huu, P. Vennegues, M. J. Ledoux and J. Guille, Physical characterization of molybdenum oxycarbide catalyst; TEM, XRD and XPS, *Catal. Today*, 1995, **23**, 251-267.

[22] S. T. Oyama, P. Delporte, C. Pham-Huu and M. J. Ledoux, Tentative structure of molybdenum oxycarbide, *Chem. Lett.*, 1997, **26**, 949-950.

[23] C. Bouchy, C. Pham-Huu, B. Heinrich, C. Chaumont and M. J. Ledoux, Microstructure and characterization of a highly selective catalyst for the isomerization of alkanes: A molybdenum oxycarbide, *J. Catal.*, 2000, **190**, 92-103.

[24] M. -L. Frauwallner, F. López-Linares, J. Lara-Romero, C. E. Scott, V. Ali, E. Hernández and P. Pereira-Almao, Toluene hydrogenation at low temperature using a molybdenum carbide catalyst, *Appl. Catal. A*, 2011, **394**, 62-70.

[25] G. Vitale, M. L. Frauwallner, E. Hernandez, C. E. Scott and P. Pereira-Almao, Low temperature synthesis of cubic molybdenum carbide catalysts via pressure induced crystallographic orientation of MoO_3 precursor, *Appl. Catal. A*, 2011, **400**, 221-229.

[26] P. Delporte, C. Pham-Huu and M. J. Ledoux, Effect of the reaction temperature and hydrocarbon partial pressure on the activity of carbon-modified MoO_3 for *n*-hexane isomerization, *Appl. Catal. A*, 1997, **149**, 151-180.

[27] A. -F. Lamic, C.-h. Shin, G. Djega-Mariadassou and C. Potvin, Characterization of new bimetallic oxycarbide ($MoWC_{0.5}O_{0.6}$) for bifunctional isomerization of n-heptane, *Catal. Lett*., 2006, **107**, 89-94.

[28] S. T. Oyama, C. C. Yu and S. Ramanathan, Transition metal bimetallic oxycarbides: synthesis, characterization, and activity studies, *J. Catal.*, 1999, **184**, 535–549.

[29] C. Bouchy, C. Pham-huu and M. J. Ledoux, On the role of hydrogen during the reduction–carburation of MoO_3 into molybdenum oxycarbide, *J. Mol. Catal. A*, 2000, **162**, 317-334.

[30] L. O. Alemán-Vázquez, E. Torres-García, J. R. Villagómez-Ibarra and J. L. Cano-Domínguez, Effect of the particle size on the activity of MoO_xC_y catalysts for the isomerization of heptane, *Catal. Lett.*, 2005, **100**, 219-226.

[31] M. J. Ledoux, P. Del Gallo, C. Pham-Huu and A. P. E. York, Molybdenum oxycarbide isomerization catalysts for cleaner fuel production, *Catal. Today*, 1996, **27**, 145-150.

[32] M. J. Ledoux, F. Meunier, B. Heinrich, C. Pham-Huu, M. E. Harlin and A. O. I. Krause, Part I. *n*-Butane dehydrogenation on unsupported carbon modified MoO_3 (MoO_xC_y): effect of steam on the catalyst stability, *Appl. Catal. A*, 1999, **181**, 157-170.

[33] T. Prasomsri, M. Shetty, K. Murugappan and Y. Roman-Leshkov, Insights into the catalytic activity and surface modification of MoO_3 during the hydrodeoxygenation of lignin-derived model compounds into aromatic hydrocarbons under low hydrogen pressures, *Energy Environ. Sci.*, 2014, **7**, 2660-2669.

[34] A. Katrib, P. Leflaive, L. Hilaire and G. Maire, Molybdenum based catalysts. I. MoO_2 as the active species in the reforming of hydrocarbons, *Catal. Lett*, 1996, **38**, 95-99.

[35] T. Matsuda, H. Shiro, H. Sakagami and N. Takahashi, Isomerization of heptane on molybdenum oxides treated with hydrogen, *Catal. Lett.*, 1997, **47**, 99-103.

[36] H. Sakagami, Y. Asano, N. Takahashi and T. Matsuda, H_2 reduction of hydrogen molybdenum bronze to porous molybdenum oxide and its catalytic properties for the conversions of pentane and propan-2-ol, *Appl. Catal. A*, 2000, **193**, 185–193.
[37] A. Mehdad, R. E. Jentoft, F. C. Jentoft, Single-phase mixed molybdenum-niobium carbides: Synthesis, characterization and multifunctional catalytic behavior in toluene, conversion, *J. Catal.*, 2017, **351**, 161–173.
[38] L. Kihlborg, *Arkiv for Kemi*, 1963, **21**, 357-364.
[39] E. Torres-García, G. Rodríguez-Gattorno, J. A. Ascencio, L. O. Alemán-Vázquez, J. L. Cano-Domínguez, A. Martínez-Hernández and P. Santiago-Jacinto, New insights on molybdenum suboxide: Nature of carbons in isomerization reactions, *J. Phys. Chem. B*, 2005, **109**, 17518-17525.
[40] I. F. Ferguson, J. B. Ainscough, D. Morse and A. W. Miller, *Nature (London)*, 1964, **202**, 1327-1328.
[41] S. G. Lias, J. F. Liebman, R.D. Levin, *J. Phys. Chem. Ref. Data* 1984, **13**, 695-808.
[42] E. P. L. Hunter and S. G. Lias, *J. Phys. Chem. Ref. Data* 1998, **27**, 413-656.
[43] D.J. Parrillo, A.T. Adamo, G.T. Kokotailo and R.J. Gorte, Amine adsorption in H-ZSM-5, *Appl. Catal.*, 1990, **67**, 107-118.
[44] A. Hanif, T. Xiao, A. P. E. York, J. Sloan and M. L. H. Green, Study on the structure and formation mechanism of molybdenum carbides, *Chem. Mater.*, 2002, **14**, 1009-1015.
[45] N. E. Fouad, Impacts of hydrogen spillover on the reduction behavior of tungsten oxide: Isothermal and non-isothermal approaches, *J. Anal. Appl. Pyrolysis*, 1997, **44**, 13–28.
[46] A. Mehdad, R. E. Jentoft, F. C. Jentoft, Single-Phase Mixed Molybdenum-Tungsten Carbides: Synthesis, Characterization and Catalytic Activity for Toluene Conversion, *Catal. Today*, https://doi.org/10.1016/j.cattod.2018.06.037.
[47] T. Xiao, A. P. E. York, K. S. Coleman, J. B. Claridge, J. Sloan, J. Charnock and M. L. H. Green, Effect of carburising agent on the structure of molybdenum carbides, *J. Mat. Chem*., 2001, **11**, 3094-3098.
[48] T. Ohno, Z. Li, N. Sakai, H. Sakagami, N. Takahashi and T. Matsuda, Heptane isomerization over molybdenum oxides obtained by H_2 reduction of H_xMoO_3 with different hydrogen contents, *Appl. Catal. A*, 2010, **389**, 52-59.
[49] H. Belatel, H. Al-Kandari, F. Al-Khorafi, A. Katrib and F. Garin, Catalytic reactions of methylcyclohexane (MCH) on partially reduced MoO_3, *Appl. Catal. A*, 2004, **275**, 141–147.
[50] G. B. McVicker, O. C. Feeley, J. J. Ziemiak, D. E. W. Vaughan, K. C. Strohmaier, W. R. Kliewer and D. P. Leta, Methylcyclohexane ring-contraction: A sensitive solid acidity and shape selectivity probe reaction, *J. Phys. Chem. B*, 2005, **109**, 2222-2226.
[51] J. R. Anderson and N. R. Avery, The mechanism of isomerization of aliphatic hydrocarbons at a platinum surface, *J. Catal.*, 1967, **7**, 315-323.
[52] M. A. Uguina, J. L. Sotelo, D. P. Serrano and J. L. Valverde, Deactivation kinetics of para-selective toluene disproportionation over modified ZSM-5, *Ind. Eng. Chem. Res.*, 1994, **33**, 26-31.
[53] D. C. Grenoble, The chemistry and catalysis of the toluene hydrodealkylation reaction: I. The specific activities and selectivities of Group VIIB and Group VIII metals supported on alumina, *J. Catal.*, 1979, **56**, 32-39.
[54] J. H. Sinfelt, Specificity in catalytic hydrogenolysis by metals, *Adv. Catal.*, 1973, **23**, 91-119.
[55] A. Gulino, T S. Parker, F. H. Jones and R. G. Egdell, Influence of metal-metal bonds on electron spectra of MoO_2 and WO_2, *J . Chem. Soc., Faraday Trans.*, 1996, **92**(12), 2137-2141.
[56] H. Belatel, H. Al-Kandari, F. Al-Kharafi, F. Garin and A. Katrib, Catalytic reactions of methylcyclohexane (MCH), on partially reduced tungsten oxide(s), *Appl. Catal. A*, 2007, **318**, 227-233.
[57] P. Del Gallo, F. Meunier, C. Pham-Huu, C. Crouzet and M. J. Ledoux, Selective *n*-butane isomerization over high specific surface area MoO_3-carbon-modified catalyst, *Ind. Eng. Chem. Res.*, 1997, **36**, 4166-4175.
[58] T. Matsuda, Y. Hirata, H. Itoh, H. Sakagami and N. Takahashi, Effect of reduction temperature on the transformation of MoO_3 to MoO_x with a large surface area, *Microporous Mesoporous Mater.*, 2001, **42**, 337-344.

[59] H. A. Benesi, Determination of proton acidity of solid catalysts by chromatographic adsorption of sterically hindered amines, *J. Catal.*, 1973, **28**, 176-178.

[60] C. Morterra, G. Cerrato and G. Meligrana, Revisiting the use of 2,6-dimethylpyridine adsorption as a probe for the acidic properties of metal oxides, *Langmuir*, 2001, **17**, 7053-7060.

[61] V. M. Whiffen, K. J. Smith, Hydrodeoxygenation of 4-methylphenol over unsupported MoP, MoS_2, and MoOx catalysts, *Energy Fuels*, 2010, **24**, 4728-4737.

[62] A. Goguet, S. Shekhtman, F. Cavallaro, C. Hardacre and F. C. Meunier, Effect of the carburization of MoO_3-based catalysts on the activity for butane hydroisomerization, *Appl. Catal. A*, 2008, **344**, 30-35.

[63] T. Matsuda, Y. Hirata, S. Suga, H. Sakagami, N. Takahashi, Effect of H_2 reduction on the catalytic properties of molybdenum oxides for the conversions of heptane and 2-propanol, *Applied Catalysis A: General*, 2000, **193**, 185–193.

[64] P. Wehrer, L. Hilaire and E. Petit, Influence of the reduction conditions of MoO_3 on its isomerizing properties, *Appl. Catal. A*, 2004, **273**, 249-258.

[65] P. Wehrer, L. Hilaire and G. Maire, About the stability of alkane isomerizing catalysts made up of molybdenum oxides, *Appl. Catal. A*, 2001, **208**, 259-264.

[66] P. Del Gallo, C. Pham-Huu, C. Bouchy, C. Estournes and M. J. Ledoux, Effect of the total activation pressure on the structural and catalytic performance of the SiC supported MoO_3-carbon-modified catalyst for the n-heptane isomerization, *Appl. Catal. A*, 1997, **156**, 131-149.

[67] H. J. Guzmán, W. Xu, D. Stacchiola, G. Vitale, C. E. Scott, J. A. Rodríguez and P. Pereira-Almao, In situ time-resolved X-ray diffraction study of the synthesis of Mo_2C with different carburization agents, *Can. J. Chem.*, 2013, **91**, 573–582.